Sequential reaction processes in the $^{12}C+^{12}C$ system at an energy of 28.7 MeV/nucleon

A. Magiera, J. Hebenstreit, L. Jarczyk, B. Kamys, A. Strzałkowski, and B. Styczeń
Institute of Physics, Jagellonian University, PL-30059 Cracow, Poland

W. Oelert, P. von Rossen, and H. Seyfarth
Institut für Kernphysik, Forschungszentrum Jülich, Federal Republic of Germany
(Received 15 May 1997)

Inclusive spectra of different ejectiles and coincidence spectra of α particles with various nuclides emerging from the collisions of ^{12}C ions of energy 344.5 MeV with a ^{12}C target have been measured. A large fraction of the observed cross section is contained in the continuous part of the inclusive spectra. In the coincidence data the excitation of states of intermediate nuclei is observed which indicates the sequential mechanism of the reaction. Calculations performed with a simple phenomenological model of such processes reproduce well the shape and magnitude of both inclusive and coincidence spectra. The contribution of various reaction mechanisms to the total reaction cross section is estimated. [S0556-2813(98)04002-3]

PACS number(s): 25.70.Mn, 25.70.Pq

I. INTRODUCTION

In the investigations of nucleus-nucleus collisions at intermediate energies large effort is concentrated on studies of the reaction mechanism leading to many-body final states. It is expected that in the beam energy range from 20 to 100 MeV/nucleon new phenomena may occur. This energy range is transitional between the low-energy regime where mean field determines the interaction process and the high-energy region where collisions of individual nucleons dominate. In the intermediate energy region a strong competition between low and high energy reaction mechanisms should appear. Therefore, besides the reaction mechanisms dominating at low energies (compound nucleus and direct reactions), other processes responsible for production of many particles in the exit channel should be regarded. Two basic, extreme models of reactions leading to a multiparticle final state are considered: the first one is a sequential binary decay—similar to that observed at low energies; the second one—predicted for large energies—corresponds to simultaneous disintegration (prompt fragmentation). A classification of various reaction mechanisms proposed for the intermediate energy region as well as a review of experimental data and different models are presented in Refs. [1] and [2]. In spite of numerous experimental investigations and a variety of proposed models for the reaction mechanism the situation is still unresolved because the performed experiments were not able to disentangle well different processes such as sequential fragmentation processes and prompt fragmentation. Moreover the models of sequential and prompt fragmentation predict a very similar behavior of different experimental observables, since their general features are governed mainly by the available phase space. While in most investigations it was found that sequential processes dominate, some authors claim observation of nonsequential processes [3–14].

In the present work measurements were performed for light system of heavy ions $^{12}C+^{12}C$ at an incident energy of 28.7 MeV/nucleon. This beam energy is high enough to induce processes different from those expected at low energies. The specific choice of entrance channel nuclei in the present experiment allows for considerable simplification of the analysis. First the study of reactions in light system of heavy ions limits the number of possible partitions in the observed final state. Secondly the identity of interacting nuclei in the entrance channel and therefore fore-aft symmetry in the center of mass frame puts very stringent constraints on the data. In such a case identical processes are responsible for production of projectilelike and targetlike nuclei. Therefore, the reactions with a many body exit channel might be measured by the observation of fragmentation products of projectile like nuclei and owing to the fore-aft symmetry by the observation of associated target like nuclei. The additional experimental advantage of using light nuclei in the entrance channel is that the reaction products are also light, what enables their detection with a low energy threshold, good mass and charge separation of ejectiles and good energy resolution. The inclusive measurements of the energy spectra and angular distributions for various ejectiles (from ^{4}He up to ^{15}N) as well as coincidence measurements in different angular configurations were performed. The differential inclusive cross sections and coincidence cross sections were extracted. That results in a large set of experimental data containing transitions to discrete bound or unbound states of ejectiles, the continuous spectra that correspond to the excitation of highly excited states of ejectiles or to many body reactions, and the correlation of two particles emitted in many body processes. The experimental data were analyzed by means of various methods. Partial analysis of the inclusive data was performed earlier and published elsewhere [15–19]. In the present paper more attention is paid to the coincidence data and simultaneous description of coincidence and inclusive distributions. The coincidence data were analyzed basing on kinematical considerations, enabling one to obtain model independent information about the reaction mechanism leading to many particles in the exit channel. The phenomenological approach was applied in the analysis of sequential decay processes initiated by the inelastic excitation and transfer reactions. More details of this analysis may be found in Ref. [20].

The experimental procedure will be presented in Sec. II together with a discussion of characteristic features of the

experimental data. The model independent qualitative discussion of the coincidence data based on the kinematical signatures of the sequential fragmentation is presented in Sec. III. The model used for the analysis of the sequential processes initiated by direct reactions is presented in Sec. IV together with the results of the phenomenological analysis of sequential fragmentation processes. In Sec. V the contribution of various reaction mechanisms is discussed and final conclusions are presented.

II. EXPERIMENTAL PROCEDURE AND RESULTS

The experiments were performed using the ^{12}C ion beam of 344.5 MeV energy from the JULIC cyclotron of the Forschungszentrum Jülich. The experiments contained measurements of the inclusive energy spectra and coincidences. The beam was focused on a ^{12}C target of 1.1 mg/cm^2 thickness. The detection system consisted of three counter telescopes assembled of 50 μm, 400 μm, 2 mm, and 6 mm thick Si surface barrier detectors cooled down to $-20\,^{\circ}$C. The solid angle covered by the detectors was 0.04 msr in inclusive experiments and 0.2 msr in coincidence measurements. This detection system is capable to separate the reaction products from ^{4}He up to ^{15}N according to their mass and charge in the energy range starting from threshold about 3–4 MeV/nucleon (see Ref. [16]). The energy resolution was 700 keV and the accuracy of the absolute energy scale was about 0.8%. The time differences of the pulses from the telescope pairs in coincidence were measured with the resolution of about 1 ns, which allowed a good discrimination against random coincidence events.

The absolute values of cross section were evaluated from the measured counting rates, target thickness, solid angles of the detecting system and integrated beam charge. The uncertainty in absolute normalization of the cross section was estimated to be 7% mainly due to the uncertainty in target thickness.

In the inclusive measurements the energy spectra of all stable ejectiles from ^{4}He up to ^{15}N were measured at laboratory angles covering the range from 4° to 11.5° in 0.5° steps and then up to 36° in 1° steps. This range covers a large part of the angular distributions. It follows from the identity of particles in the entrance channel that the cross section is symmetrical around 90° in the center of mass system (this corresponds to about 45° in the laboratory system).

The coincidences of various ejectiles were measured for angular configurations in a ''close geometry'' $(+6°,-6°)$, $(+6°,+11°)$ and in a ''wide geometry'' $(+6°,-20°)$, $(+6°,-30°)$. All telescopes were placed in the plane including the beam direction. The same sign of the angles refers to telescopes placed on the same side of the beam and different signs correspond to telescopes placed on opposite sides of the beam. In the angular settings chosen for the coincidence measurements one of the telescopes was always placed at small angle $+6°$. This telescope enables to detect the ejectiles produced in processes which are peaked at forward angles. Positions of the second detector cover the large part of the angular range.

The high energy part of the spectra where discrete peaks were observed was additionally measured using the Big Karl spectrometer. This allowed a better resolution of the transitions to discrete states (with energy resolution of about 200 keV) and a measurement at small angles down to 2°. The spectrometer was used also for the measurement of the Rutherford elastic scattering at small angles on a ^{197}Au target to verify the absolute normalization of the cross section.

More details about the experimental procedure, particle identification and results for inclusive measurements may be found in Refs. [16] and [20]. Typical measured inclusive energy spectra could be found also there. The spectra at forward angles are dominated by the broad maximum located at energies close to those corresponding to the beam velocity. This maximum is asymmetric with a tail extending to small ejectile energies. At larger angles this maximum practically disappears and spectra decrease strongly with the ejectile energy. At small energies where the contribution from the compound nucleus reaction may be expected the observed cross section is small. The transitions to discrete states with definite excitation energies are observed for some ejectiles [18]. They appear distinctly at small detection angles only. Such transitions to discrete states correspond to inelastic scattering and one- and two-nucleon transfer reactions.

The typical coincidence patterns are shown in Fig. 1 as a two dimensional scatter plot of the intensity in function of the energies of the coincident fragments for a given angular configuration. The coincidence spectra presented in Figs. 1(a) and 1(b) are for ''close geometry,'' i.e., angle settings $(+6°,+11°)$ and coincidences of $\alpha-{}^9$Be and $\alpha-{}^6$Li, respectively, that in Fig. 1(c) is for ''wide geometry'' angular setting, i.e., $(+6°,-30°)$ for coincidences of $\alpha-{}^6$Li. The kinematical curves calculated from energy and momentum conservation for the corresponding three body reaction ^{12}C(^{12}C,α^9Be)^{11}C for $\alpha-{}^9$Be and ^{12}C(^{12}C,α^6Li)^{14}N for $\alpha-{}^6$Li coincidences are also plotted. These curves define the limits for the kinetic energy of particles in coincidence. The events situated on the kinematical curve correspond to the three body reaction with all particles in the ground state. Events lying inside the region enclosed by this curve may be accounted to the excitation of ejectiles or to more than three body reactions. Events above this region correspond to random coincidences only.

As it is seen from Fig. 1 qualitatively different coincidence patterns are observed in these three cases. In Fig. 1(a) the majority of the coincidence events is concentrated close to the kinematical curve calculated for the ^{12}C(^{12}C,α^9Be)^{11}C three-body reaction with all ejectiles in the ground states. Beyond the vicinity of kinematical curve some events are observed at ejectile energies smaller than those on the kinematical curve. This type of coincidence pattern is dominating for $\alpha+{}^9$Be and $\alpha+{}^{10}$B coincidences in ''close geometry.'' The second type of observed coincidence pattern is presented in Fig. 1(b). It is characterized by majority of coincidence events with ejectile energies much smaller than those corresponding to the kinematical curve. These coincidence events are, however, not distributed randomly but they are correlated to some curves. Similar behavior of the coincidence cross section is observed also for $\alpha-{}^7$Be, $\alpha-{}^7$Li, $\alpha-{}^6$Li, and $\alpha-\alpha$ coincidences in ''close geometry.'' The third type of coincidence pattern appears for ''wide geometry.'' As may be seen in Fig. 1(c) the coincidence events are concentrated at small energies of both detected ejectiles. They do not group close to the kinematical

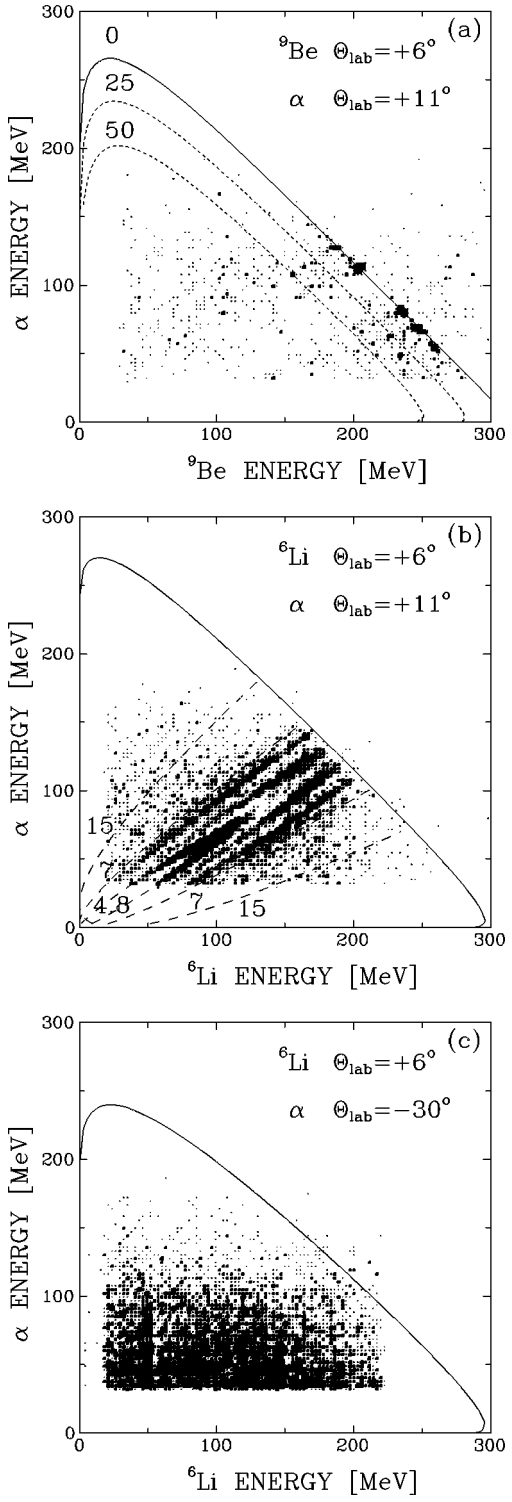

FIG. 1. Two-dimensional spectrum for $\alpha - {}^9$Be (a) and $\alpha - {}^6$Li (b) coincidences for an angular configuration $(+6°, +11°)$ and for $\alpha - {}^6$Li (c) for angular configuration $(+6°, -30°)$. The density of the points corresponds to the magnitude of the cross section and varies logarithmically. The solid curve represents the ejectile energies that correspond to a three body reaction with all final state particles in their ground states (kinematical curve). The kinematical curves for various values of missing energy Q_3 (dotted lines) and some selected values of excitation energy E^*_{12} (dashed lines) are also shown. Numbers labeling the curves correspond to Q_3 and E^*_{12} values in MeV.

curves as for ''close geometry.'' For the ''wide geometry'' the patterns for all coincidences of α particle with heavier ejectile are very similar.

III. ANALYSIS OF COMPOUND NUCLEUS, INELASTIC EXCITATION, AND TRANSFER REACTIONS

At small incident energies for the light systems of heavy ions (e.g., $^{12}C+{}^{12}C$ system) reactions are dominated by compound nucleus and direct processes (i.e., inelastic scattering and transfer reactions). Both these processes contribute also to the continuous part of the spectra. The compound nucleus contribution is expected at energies corresponding to the center of mass velocity, while for direct reactions—close to the beam velocity. The contributions of these well known mechanisms have to be regarded before other reaction mechanisms that may appear at intermediate energy are considered.

A. Compound nucleus reactions

To evaluate the contribution of the compound nucleus reaction to the spectra of various ejectiles the calculations of particle evaporation from the compound nucleus were performed using the PACE code [21]. The resulting cross section depends on the parameters in the level density formula and on the maximum angular momentum l_f for fusion.

For the calculations of the level density the Gilbert-Cameron parameterization [22] was used. It contains two basic parameters: the level density parameter a and the pairing energy. The level density parameter used usually for light nuclei $a=A/5$ (A is the nucleus mass number) and the pairing energy parameterization proposed in Ref. [23] were applied. The same parameters were successfully used in an extended analysis of $^9Be+{}^{12}C$ fusion at $E_{c.m.}=11.4$ MeV [24] and $^{11}B+{}^{12}C$ fusion at $E_{c.m.}=36.5$ and 41.7 MeV [25], where the same nuclei as in the present analysis appear in the compound nucleus decay.

The potential model (Refs. [26,27]) was used to estimate the maximum angular momentum for fusion. According to this model l_f corresponds to the angular momentum l_{crit} for which the ''pocket'' in the total potential (Coulomb, nuclear, and centrifugal) disappears. Using the optical model potential determined for $^{12}C+{}^{12}C$ system [15] value of $l_f=l_{crit}=17$ was obtained. This value leads to a fusion cross section of 200 mb in good agreement with the predictions of the Porto-Sambataro phenomenological model [28] resulting in a fusion cross section value equal to 180 mb. The total reaction cross section amounts to 1290 mb.

As an example the results of these calculations for ^{10}B and α particle ejectiles are compared with the experimental energy spectra in Fig. 2 for some angles. The obtained cross section for the outgoing ^{10}B produced as an evaporation residuum accounts for a considerable portion of the experimental cross section at small ejectile energies and small angles only. The contribution of the evaporation residuum cross section decreases with increasing angle and becomes very small in respect to the experimental cross section at laboratory angles larger than 25°. A similar behavior is observed for all other evaporation residua. As shown in Figs. 2(c) and 2(d) the cross section for α particles evaporated in

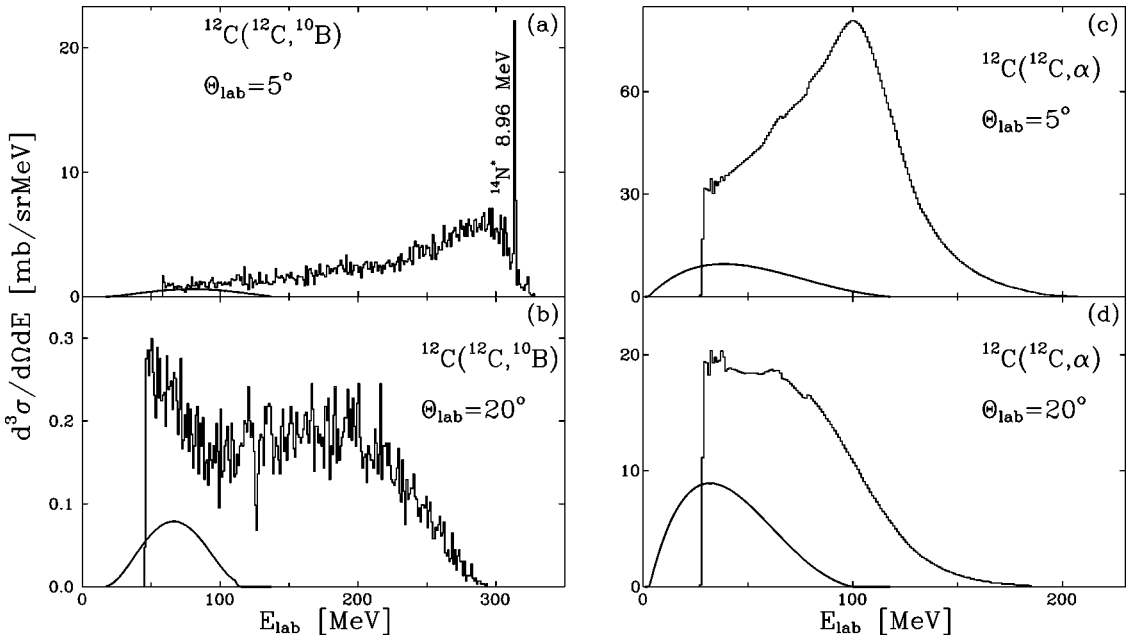

FIG. 2. Energy distributions (histograms) of outgoing ^{10}B nuclei and α particles for selected angles compared with statistical model calculations (continuous solid line).

the decay of the compound nucleus is very small in comparison to the experimental data at small angles, while it increases to about 20% of the experimental cross section at larger angles.

B. Direct reaction processes

For the investigated system the direct reactions leading to bound and a continuum of unbound states were calculated [15,18,19]. The inelastic excitation [15] and transfer reactions to discrete states [18] were analyzed within the standard DWBA. Very good reproduction of the experimental angular distributions was obtained, and the values of the potential deformation length and spectroscopic factors agree very well with those from the other studies at low incident energies for various systems. The inelastic excitations to higher excited states were calculated [19] with the multistep direct reaction (MSDR) model (see Fig. 3). It was shown that inelastic scattering and transfer reactions are still quite important at intermediate beam energy. They account for the observed transitions to discrete states and for a part of the continuum spectra for ^{12}C nuclei (inelastic excitation) and ^{11}C and ^{11}B ejectiles (transfer reactions) at large outgoing energies. Such direct reactions leading to unbound states initialize the sequential processes.

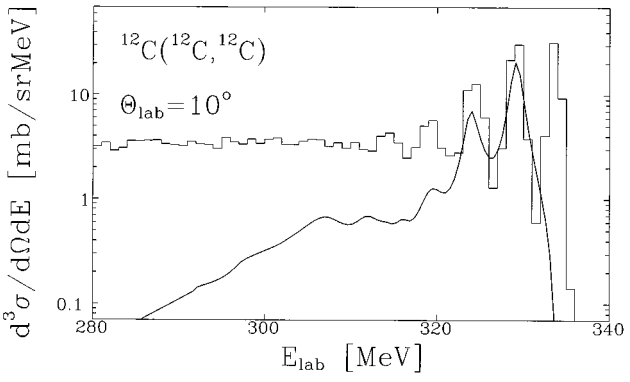

FIG. 3. Energy distributions of outgoing ^{12}C nuclei at a laboratory angle of 10°. The thick solid line corresponds to MSDR calculations of inelastic processes. The peak at the largest energy corresponds to the elastic scattering (figure from [19]).

The excitation of the 8.96 MeV state of ^{14}N in deuteron transfer reaction and its subsequent proton decay may be regarded as a good example of such a sequential process. This process is shown schematically in Fig. 4. The deuteron transfer to the ^{14}N 8.96 MeV state leads to a strong peak in ^{10}B spectrum presented in Fig. 2(a). This state is unbound and decays by proton emission with 100% probability since other decay channels are closed as their energy thresholds are larger than 9 MeV. Because of identical particles in the entrance channel it is possible to obtain directly the cross section for both ^{10}B and ^{14}N* outgoing particles by detecting ^{10}B ejectiles only. The identity of entrance channel particles results also in the fore-aft symmetry of the cross section in the center of mass system. Thus in the example shown in Fig. 4 the cross sections for the production of ^{10}B and ^{14}N* ejectiles are equal for given c.m. angle:

$$\frac{d\sigma_{^{10}B}(\theta_{\text{c.m.}})}{d\Omega_{\text{c.m.}}}=\frac{d\sigma_{^{10}B}(\pi-\theta_{\text{c.m.}})}{d\Omega_{\text{c.m.}}}=\frac{d\sigma_{^{14}N*}(\theta_{\text{c.m.}})}{d\Omega_{\text{c.m.}}}.$$

Therefore the angular distribution measured for the tran-

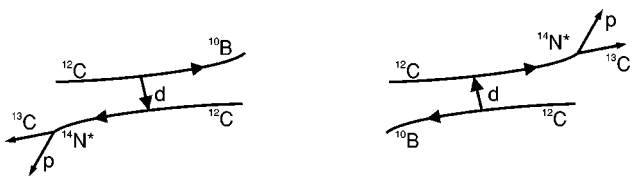

FIG. 4. Schematic representation of the deuteron transfer reaction $^{12}C+^{12}C\rightarrow^{10}B+^{14}N^*$ with a subsequent proton decay of excited state of $^{14}N^*\rightarrow p+^{13}C$.

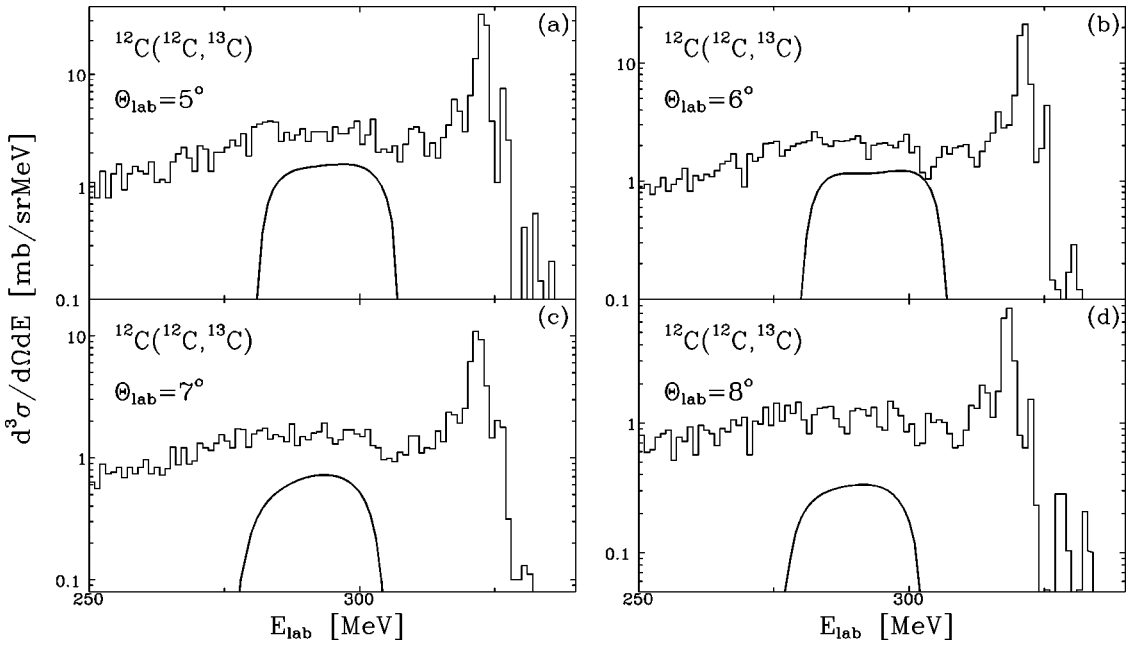

FIG. 5. The experimental energy spectra for outgoing ^{13}C compared with sequential process calculations (solid line) as described in the text.

sitions corresponding to the peak in ^{10}B spectra could be used to obtain the formation probability of $^{14}N^*$ nucleus emitted in the forward hemisphere in the first stage of the reaction. Assuming that the decay is isotropic in the rest frame of the $^{14}N^*$ nucleus the cross section for outgoing ^{13}C nuclei produced in a sequential decay process can be calculated without free parameters. The results of these calculations with intermediate 8.96 MeV state of $^{14}N^*$ nucleus are presented in Fig. 5. In the kinematically allowed region the contribution of the sequential process, described above, to the continuous part of ^{13}C spectra is significant. That indicates the importance of the sequential processes initiated by direct reactions leading to unbound states. At larger angles the calculated cross section accounts only for a small part of the experimental cross section for the ^{13}C nucleus. This suggests that transitions to higher excited states of the ^{14}N nucleus have to be considered. Higher excited levels decay in the laboratory system into a larger angular cone. Therefore they contribute significantly at larger emission angles, and consequently their decay leads to a broader laboratory energy distributions of ejectiles.

IV. KINEMATICAL SIGNATURES OF THE SEQUENTIAL FRAGMENTATION REACTIONS

As shown in the previous section various processes like compound nucleus formation and decay as well as direct and sequential reactions lead to continuous distributions in the inclusive spectra. They can be only distinguished by appropriate model calculations. Since the coincidence data contain more information than the inclusive ones it may be expected, that some model independent conclusions about the reaction mechanism may be drawn from their analysis. For this purpose the characteristic features of the measured coincidence patterns will be discussed based only on kinematical considerations.

The energies of the two outgoing particles detected in coincidence at given emission angles were measured in the present experiment. The distribution of points in the scatter plot (energy of the first particle versus energy of the second one) is determined just by the phase space factor in case of uncorrelated particles. Deviation from the resulting smooth distribution indicates the presence of some dynamical correlations, thus it should contain information on the reaction mechanism. This will be most clearly visible when representing the coincidence cross section as a function of two variables: excitation energy E_{12}^* of the subsystem consisting of two observed particles, and the missing energy Q_3, i.e., the energy of unobserved particles.

For the coincidences of ejectiles 1 and 2 (with known masses m_1 and m_2 and four momenta p_1 and p_2) emerging from the interaction of beam particles ''a'' with target nuclei ''b,'' these variables have the following definition:

$$E_{12}^*=\sqrt{(p_1+p_2)^2}-m_{12},$$

where m_{12} is the ground state mass of the nucleus formed of nucleons of particle 1 and 2:

$$Q_3=\sqrt{p_x^2}-m_x=\sqrt{(p_a+p_b-p_1-p_2)^2}-m_x,$$

where p_x is the four momentum of all unobserved particles ($p_x=p_3+\cdots+p_n$) and m_x is the mass of the particular system of unobserved particles.

When particles 1 and 2 form a resonant state of the composed system, a peak should be visible in the coincidence cross section at the excitation energy E_{12}^* corresponding to this resonant state. The missing energy Q_3 corresponds to the excitation energy of the third, unobserved particle in a three body reaction while it corresponds to kinetic energies and excitation energies of unobserved ejectiles in case of more than three body processes. In Fig. 1 the example of contour

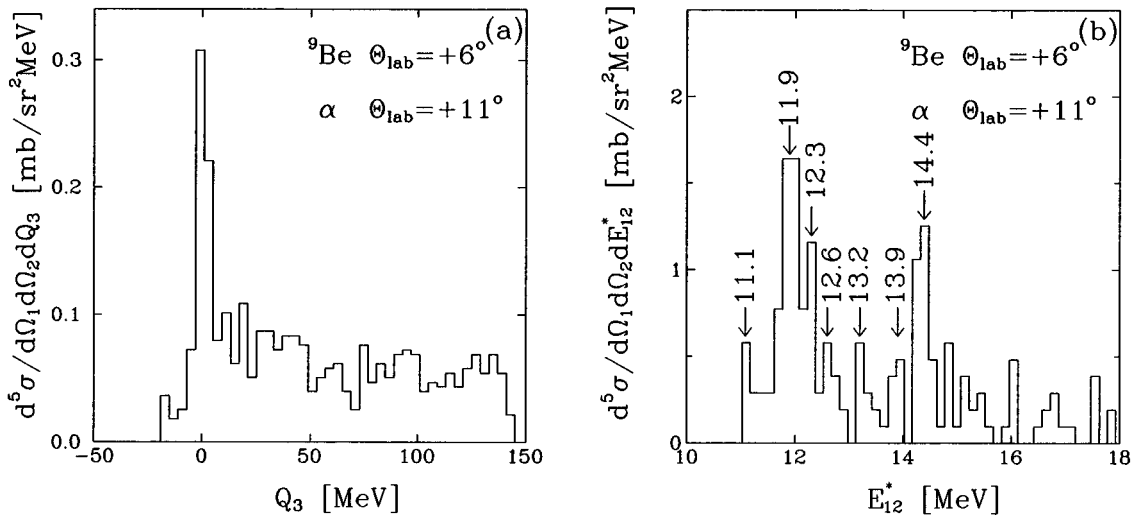

FIG. 6. Experimental coincidence cross section for $\alpha - ^9$Be coincidences presented as a function of Q_3 (a) and as a function of excitation energy E^*_{12} (b). Arrows in (b) mark the peaks corresponding to the excited states of ^{13}C nucleus, the labels above arrows indicate the values of excitation energy.

lines of excitation energy E^*_{12} and missing energy Q_3 is presented for the detection of ^{9}Be or ^{6}Li and α particle in coincidence at the angular configuration $(+6°, +11°)$.

Comparison of contour lines of E^*_{12} and Q_3 with experimental coincidence patterns leads to straightforward interpretation of the correlated structures visible in the experimental plots presented in Figs. 1(a) and 1(b). Groups of points lying on the kinematical curve of the three body reaction presented in Fig. 1(a) correspond to a missing energy equal to zero, i.e., to a three body reaction in which all ejectiles are in the ground state. These groups of points correspond, however, to well defined values of the excitation energy of a system composed of two observed particles. Thus the studied three body reaction proceeds via a sequential mechanism with excitation of states of intermediate ^{13}C system. Figure 1(b) displays another correlation pattern. The events are grouped along contour lines of constant excitation energies E^*_{12} of ^{10}B. Occurrence of different missing energy is an indication of a sequential process with more than three ejectiles in the exit channel.

It should be emphasized that the distribution of points in the scatter plot is significantly modified by the efficiency of the detection system. The efficiency is determined by the angular configuration and the solid angles of the detectors, relative velocity and the sum of the velocities of the particles detected in coincidence, hence it depends on E^*_{12}. The efficiency was calculated for each analyzed angular configuration using the Monte Carlo method. The efficiency strongly decreases with increasing E^*_{12} value and for various angular configurations the maximum of the efficiency corresponds to different E^*_{12} values. The efficiency does not depend strongly on the missing energy Q_3 and is practically constant in the whole available Q_3 range. Coincidence spectra of the $\alpha - ^9$Be and $\alpha - ^6$Li will be discussed as typical examples of a kinematical analysis.

$\alpha - ^9$Be coincidences. Figure 1(a) shows that most of the coincidence events are concentrated on the kinematical curve corresponding to $\alpha + ^9$Be$+ ^{11}$C final state with all outgoing particles in the ground state $(Q_3 = 0)$. This is well visible when the coincidence spectra are presented as function of missing energy E^*_{12} [Fig. 6(a)]. The presence of groups of points corresponding to well defined excitation energies of nucleus ^{13}C, decaying to ^{9}Be and α, indicates that the reaction proceeds sequentially with excitation of ^{13}C to several unbound states. This is illustrated in Fig. 6(b) where the projection onto E^*_{12} excitation energy of coincidence events corresponding to the peak at $Q_3 = 0$ in Fig. 6(a) is presented. The excitation of the following unbound states: 11.1, 11.9, 12.3, 12.6, 13.2, 13.9, and 14.4 MeV is visible well above the random coincidences. The continuous part of the missing energy spectrum [Fig. 6(a)] may be attributed to more than three body reactions, e.g., a four body reaction leading to $\alpha + ^9$Be$+ p + ^{10}$B final state.

According to the discussion presented above, the detection efficiency causes that only a small range of ^{13}C excitation energy may be observed for each angular configuration of detectors. Thus, to determine the excitation probability of ^{13}C nucleus in a broad energy range one has to combine the information from several angular configurations and correct it for the detection efficiency. Such an excitation probability is shown in Fig. 7. It is seen that the cross section depends exponentially on the excitation energy E^*_{12}. This dependence as well as the magnitude of the excitation probability is very similar for different angular configurations. It should be noted that these coincidence spectra contain information not only on the formation of intermediate excited states but also on the probability of their decay into $\alpha + ^9$Be channel.

$\alpha - ^6$Li coincidences. Another type of coincidence pattern is shown in Fig. 1(b). The events are grouped on curves of constant E^*_{12}, corresponding however, to a broad range of missing energy. Therefore, it may be concluded that other reactions with more than three bodies in exit channel with excitation of intermediate ^{10}B nuclei are responsible for these coincidences. The reaction may proceed via inelastic excitation of ^{12}C and its subsequent decay with emission of deuteron (or $n + p$ sequences) and α particle. Another type of the reaction mechanism leading to $\alpha - ^6$Li coincidences corresponds to alpha particle decay of excited ^{12}C with for-

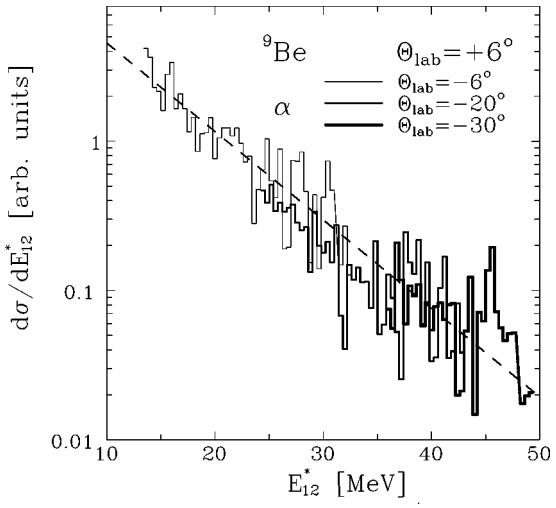

FIG. 7. Experimental coincidence spectra corrected for the detection efficiency for $\alpha - ^9$Be coincidences in different angular configurations presented as a function of the excitation energy E^*_{12}. Dashed line corresponds to an exponential function fitted using the least square method.

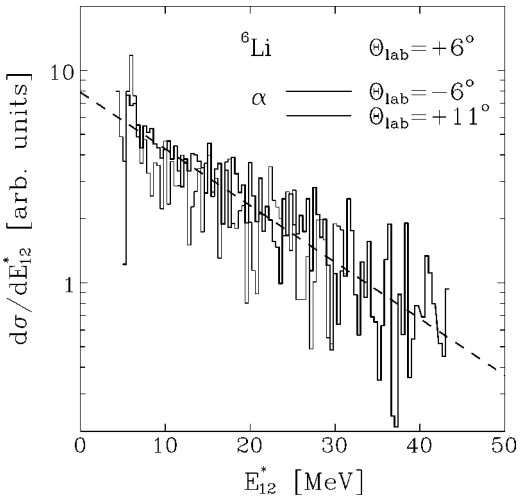

FIG. 9. Experimental coincidence spectra corrected for the detection efficiency for $\alpha - ^6$Li coincidences in different angular configurations as a function of excitation energy E^*_{12}. Dashed line corresponds to the exponential function fitted using the least square method.

mation of ^{8}Be and its successive decay into a deuteron and ^{6}Li. In this reaction the α particle and ^{6}Li are not correlated to some particular relative energy since they do not form an intermediate state. Therefore in this case the coincidence events should have a continuous distribution.

The excitation of ^{10}B levels is well visible in Fig. 8 where the $\alpha - ^6$Li coincidence cross section is presented as function of E^*_{12}. The observed peaks may be identified as corresponding to the following known ^{10}B excited states: 4.774 MeV, three unresolved states at about 5.15 MeV and a group of three states at about 6 MeV. No significant continuous contribution is observed which should appear in case of an α-deuteron decay sequence. Suppression of the reaction involving the α-deuteron sequence is due to the ^{8}Be structure which favours $\alpha - \alpha$ decay of this nucleus.

In order to obtain the excitation energy distribution of ^{10}B nuclei produced in the ^{12}C decay, the experimental $\alpha - ^6$Li

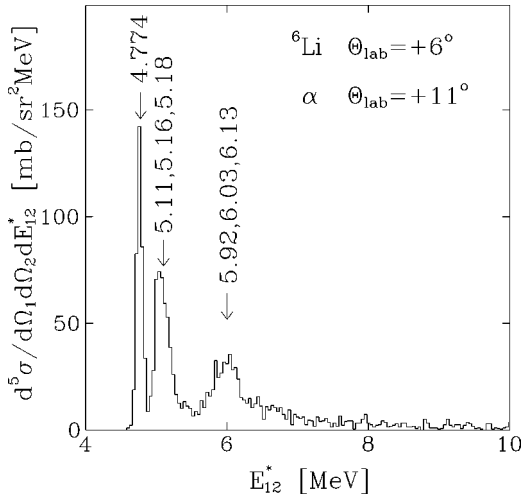

FIG. 8. Experimental coincidence cross section for $\alpha - ^6$Li coincidences as a function of excitation energy E^*_{12}. Arrows mark the peaks corresponding to the excited states of ^{10}B nucleus, the labels above arrows indicate the excitation energy.

coincidence distributions were corrected for detection efficiency. The corrected coincidence cross sections are shown in Fig. 9 for the $(+6°,-6°)$ and the $(+6°,+11°)$ angular configuration as a function of E^*_{12}. It is seen that the probability distributions of excitation energy of ^{10}B nuclei (decaying subsequently via α particle emission) are exponentially decreasing functions, similar in shape and magnitude for both angular configurations.

Since the coincidence patterns of $\alpha - ^7$Be and $\alpha - ^7$Li are analogous to those of $\alpha - ^6$Li coincidences, it may be concluded that the mechanism responsible for populating these three channels is very similar. The occupation of ^{7}Li and ^{7}Be channels is caused by sequential reactions consisting of the excitation of ^{12}C nucleus to unbound states, followed by nucleon emission populating unbound states of ^{11}C or ^{11}B, and subsequent α-particle emission. The exponential dependence on E^*_{12} of the probability of production and α particle decay of intermediate ^{11}C and ^{11}B nuclei was found from experimental coincidence spectra corrected for detection efficiency. The slope of these corrected $\alpha - ^7$Be and $\alpha - ^7$Li spectra, represented as function of E^*_{12}, is the same as that observed for $\alpha - ^6$Li coincidences.

V. SIMPLE MODEL FOR SEQUENTIAL PROCESS CALCULATIONS

As it was shown in the previous chapter the direct reactions lead frequently to unbound states which subsequently decay by particle emission. It follows from the analysis of the coincidence data, that most of the observed coincidences may originate from such sequential reactions. In this chapter it will be shown how the observed spectra may be described by a simple phenomenological model based on this reaction mechanism.

In general, the inclusive and coincidence differential cross sections are calculated by integrating the product of the transition probability $\mathcal{P}$ and the phase space density factor over all allowed values of momenta of unobserved particles. The

TABLE I. The decay channels taken into account in the calculations of the sequential processes started by inelastic excitation and one and two nucleon transfer processes. The total cross section resulting from the comparison of the calculations with experimental data is also shown for each regarded process.

Primary nucleus	Decay channel	σ_{tot} [mb]
^{12}C	$^{12}\text{C}\rightarrow n+{}^{11}\text{C}$	37
	$^{12}\text{C}\rightarrow p+{}^{11}\text{B}$	52
	$^{12}\text{C}\rightarrow d+{}^{10}\text{B}$	55
	$^{12}\text{C}\rightarrow \begin{cases} n+{}^{11}\text{C}\rightarrow n+p+{}^{10}\text{B} \\ p+{}^{11}\text{B}\rightarrow p+n+{}^{10}\text{B} \end{cases}$	38
	$^{12}\text{C}\rightarrow {}^{3}\text{He}+{}^{9}\text{Be}$	16
	$^{12}\text{C}\rightarrow n+{}^{11}\text{C}\rightarrow n+\alpha+{}^{7}\text{Be}$	44
	$^{12}\text{C}\rightarrow p+{}^{11}\text{B}\rightarrow p+\alpha+{}^{7}\text{Li}$	50
	$^{12}\text{C}\rightarrow d+{}^{10}\text{B}\rightarrow d+\alpha+{}^{6}\text{Li}$	53
	$^{12}\text{C}\rightarrow \begin{cases} n+{}^{11}\text{C}\rightarrow n+p+{}^{10}\text{B} \\ p+{}^{11}\text{B}\rightarrow p+n+{}^{10}\text{B} \end{cases} \rightarrow n+p+\alpha+{}^{6}\text{Li}$	43
	$^{12}\text{C}\rightarrow \alpha+{}^{8}\text{Be}\rightarrow \alpha+\alpha+\alpha$	392
^{13}C	$^{13}\text{C}\rightarrow n+{}^{12}\text{C}$	73
^{13}N	$^{13}\text{N}\rightarrow p+{}^{12}\text{C}$	
^{13}C	$^{13}\text{C}\rightarrow n+{}^{12}\text{C}\rightarrow n+n+{}^{11}\text{C}$	26
^{13}N	$^{13}\text{N}\rightarrow p+{}^{12}\text{C}\rightarrow p+n+{}^{11}\text{C}$	
^{13}C	$^{13}\text{C}\rightarrow n+{}^{12}\text{C}\rightarrow n+p+{}^{11}\text{B}$	43
^{13}N	$^{13}\text{N}\rightarrow p+{}^{12}\text{C}\rightarrow p+p+{}^{11}\text{B}$	
^{13}C	$^{13}\text{C}\rightarrow \alpha+{}^{9}\text{Be}$	3
^{13}C	$^{13}\text{C}\rightarrow n+n+{}^{11}\text{C}\rightarrow n+n+\alpha+{}^{7}\text{Be}$	16
^{13}N	$^{13}\text{N}\rightarrow n+p+{}^{11}\text{C}\rightarrow n+p+\alpha+{}^{7}\text{Be}$	
^{13}C	$^{13}\text{C}\rightarrow n+p+{}^{11}\text{B}\rightarrow n+p+\alpha+{}^{7}\text{Li}$	23
^{13}N	$^{13}\text{N}\rightarrow p+p+{}^{11}\text{B}\rightarrow p+p+\alpha+{}^{7}\text{Li}$	
^{14}N	$^{14}\text{N}\rightarrow \alpha+{}^{10}\text{B}$	3
	$^{14}\text{N}\rightarrow p+{}^{13}\text{C}\rightarrow p+\alpha+{}^{9}\text{Be}$	17

transition probability contains full information concerning the dynamics of the reaction while the phase space density factor corresponds to the number of available states in the exit channel while ensuring conservation of total energy and momentum. The inclusive cross section for the observed particle ''1'' may be represented as

$$2E_1\frac{d^3\sigma_n}{d^3p_1}=\frac{1}{F}\int\prod_{i=2}^{n}\frac{d^3p_i}{2E_i}\,\delta^4\left(p_a+p_b-p_1-\sum_{j=2}^{n}p_j\right)\times\mathcal{P}(\vec{p_1},\vec{p_2},\ldots,\vec{p_n})$$

and the coincidence cross section for the observed particles ''1'' and ''2'' as

$$4E_1E_2\frac{d^6\sigma_n}{d^3p_1d^3p_2}=\frac{1}{F}\int\prod_{i=3}^{n}\frac{d^3p_i}{2E_i}\times\delta^4\left(p_a+p_b-p_1-p_2-\sum_{j=3}^{n}p_j\right)\times\mathcal{P}(\vec{p_1},\vec{p_2},\ldots,\vec{p_n}),$$

where E_i, $\vec{p_i}$, p_i denote the total energy, momentum and four momentum of particle i ($i=a,b,1,2,\ldots,n$ for beam, target, and outgoing particles $1,2,\ldots,n$, respectively), F is the normalization factor corresponding to the flux of the incident particles, $d^3p_i/2E_i$ is the phase space density for particle i, and $\mathcal{P}$ corresponds to the transition probability to the exit channel with outgoing particles $1,2,\ldots,n$.

It is assumed that the formation of excited nuclei and their subsequent decays are separated in time well enough to assure that formation and decay processes are independent. Then the transition probability may be represented as a product of formation probability of excited intermediate nuclei and the probability of their successive decays. The formation probability depends on the emission angle and excitation energy of the first step reaction products while the decay probability is determined by excitation energies of the decaying nuclei and decay products. The decay probability may depend also on the emission angles when the decaying nuclei are polarized. It is, however, justified to assume that the average polarization of intermediate nuclei vanishes since many unbound states are excited in the energy region under consideration. This averaging leads to isotropic emission of the decay products in the rest frame of the decaying nuclei.

The exponential angular dependence of the transition probability on the center of mass angle $\theta_{\text{c.m.}}$ of a projectile-

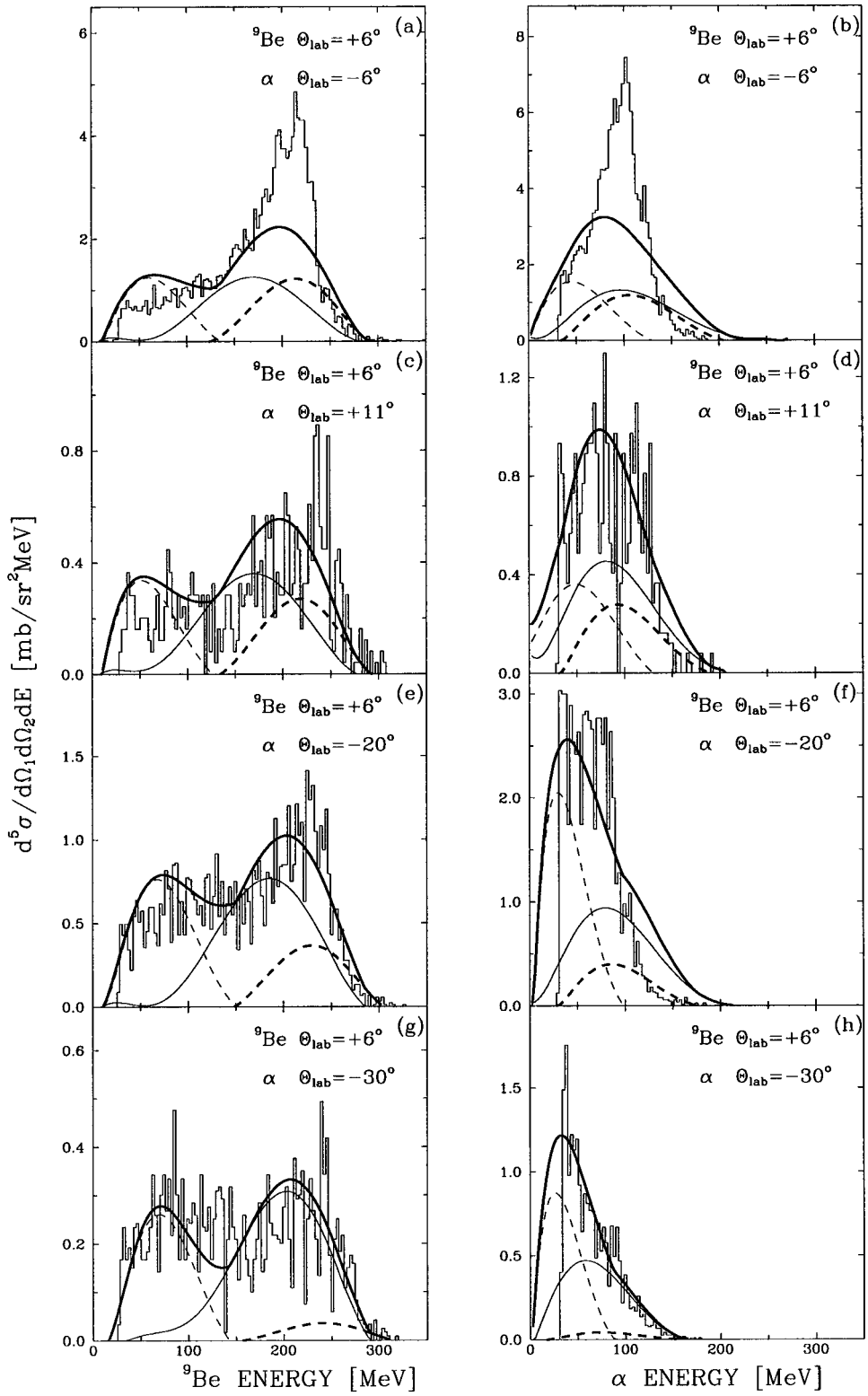

FIG. 10. Experimental $\alpha - {}^9$Be coincidence spectra compared with a sequential processes calculation ($\alpha + {}^9\mathrm{Be} + {}^{11}\mathrm{C}$, thick dashed lines; $\alpha + {}^9\mathrm{Be} + p + {}^{10}\mathrm{B}$, thin solid lines), compound nucleus calculations (thin dashed lines), and sum of all these processes (thick solid lines).

like fragment was assumed in accordance with the observed shape of angular distributions for inelastic and transfer reactions. The identity of particles in the entrance channel was taken into account by representing the transition probability as a sum of contributions for center of mass angles $\theta_{\mathrm{c.m.}}$ and $\pi - \theta_{\mathrm{c.m.}}$.

It follows from the kinematical analysis of the coincidence data for three body reactions that the formation prob-

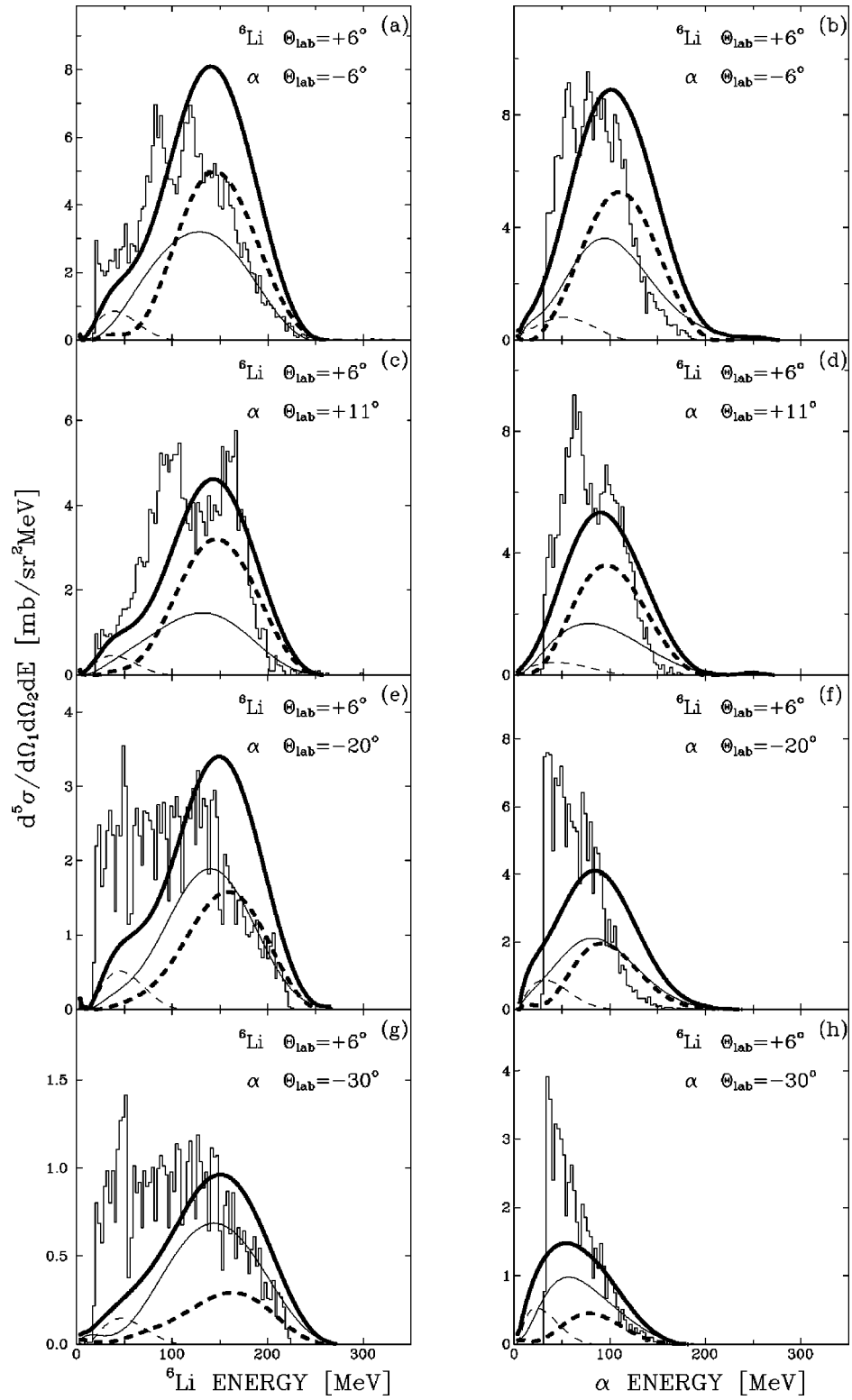

FIG. 11. Experimental $\alpha - ^6$Li coincidence spectra compared with calculations of various processes. Thick dashed lines: sequential process leading to $\alpha + ^6\mathrm{Li} + d + ^{12}\mathrm{C}$; thin solid lines: sequential process leading to $\alpha + ^6\mathrm{Li} + n + p + ^{12}\mathrm{C}$; thin dashed lines: compound nucleus calculations; thick solid lines: the sum of all these processes.

ability is an exponential function of the excitation energy E_1^* of the unstable nucleus formed in the first step of the reaction (see Fig. 7). The analysis of four body reactions (presented in Fig. 9) leads to the conclusion that the transition probability also depends exponentially on excitation energy E_2^* of the intermediate states formed in the second step of the reaction. Thus the exponential dependence of the transition probability on excitation energies of all intermediate states was assumed.

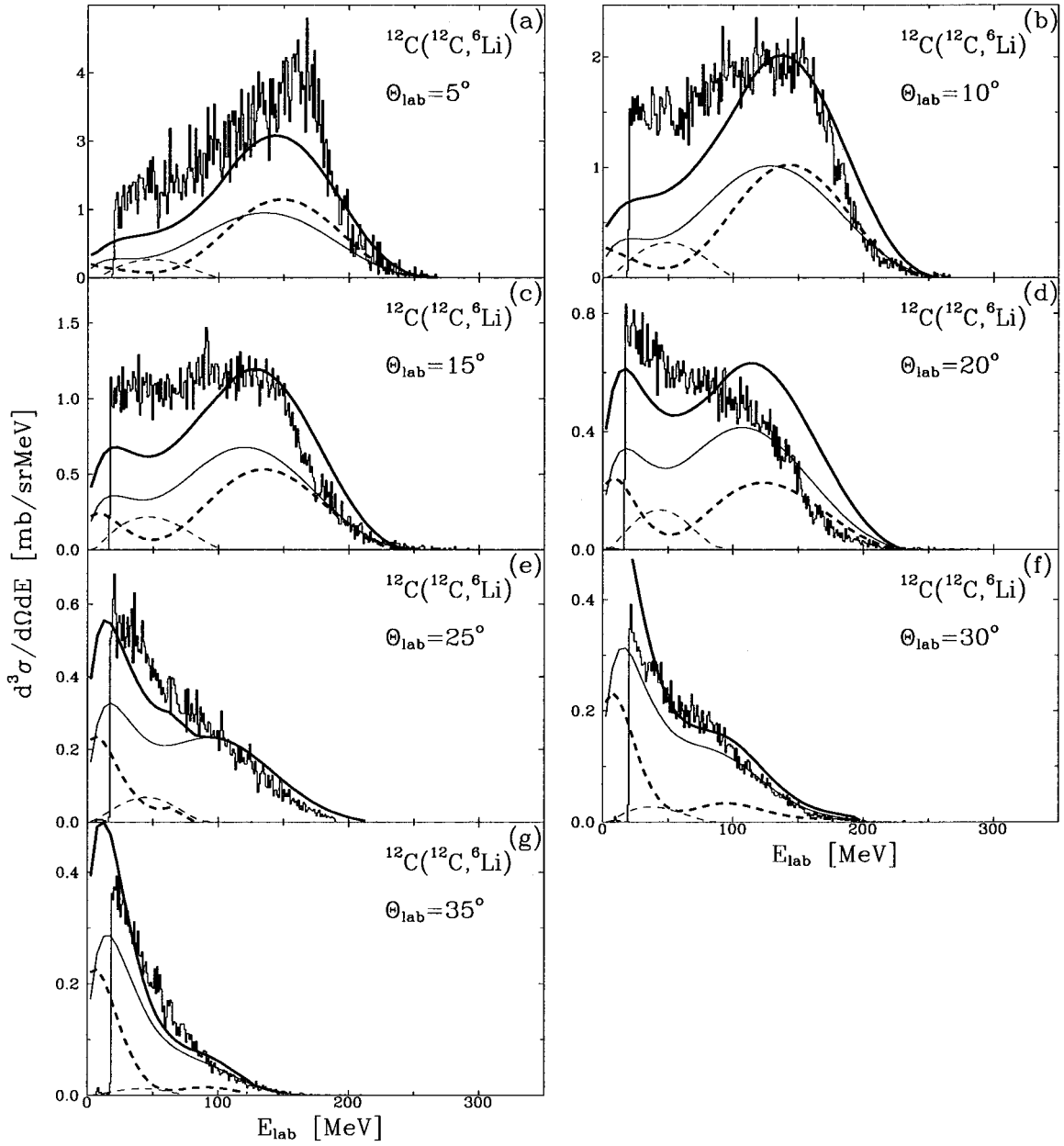

FIG. 12. Experimental ^{6}Li inclusive spectra for various laboratory angles compared with calculations. Thick dashed lines: sequential process leading to $\alpha+{}^{6}\mathrm{Li}+d+{}^{12}\mathrm{C}$; thin solid lines: processes leading to $\alpha+{}^{6}\mathrm{Li}+n+p+{}^{12}\mathrm{C}$; thin dashed lines: compound nucleus calculations. Thick solid lines represent a sum of all these processes.

Then the transition probability $\mathcal{P}$ may be written as

$$\mathcal{P}=N\cdot[\exp(-\beta\theta_{\mathrm{c.m.}})+\exp(-\beta(\pi-\theta_{\mathrm{c.m.}}))]\cdot\exp(-\gamma E_1^*-\delta E_2^*\ldots-\epsilon E_{n-1}^*-\zeta E_n^*),$$

where N is the normalization factor (different for each reaction channel), β parameter determines the slope of the angular distributions, and the parameters $\gamma, \delta, \ldots, \epsilon$ and ζ contain both probabilities of formation and decay of the excited states.

The value of the parameter β varying in the range of $0.1-0.2$ deg^{-1} was deduced from experimental and theoretical angular distributions for direct processes discussed in Sec. III B. The reproduction of experimental data was of similar quality for all values of β in this range. Therefore, the parameter β was kept constant at a value of 0.15 deg^{-1} for all calculations in the present analysis.

It was found that transfer and inelastic excitation processes exhibit a different dependence on the excitation energy of the intermediate nuclei formed in the first step of the reaction. Therefore the γ parameter was fixed at different values for sequential processes initiated by transfer and those initiated by inelastic excitation. The parameter $\gamma_{\mathrm{trans.}}=0.13$ MeV^{-1} was obtained from the analysis of the experimental coincidence spectra for three body reactions leading to $\alpha-{}^{9}\mathrm{Be}$ and $\alpha-{}^{10}\mathrm{B}$ coincidences. The parameter $\gamma_{\mathrm{inel.}}=0.04$ MeV^{-1} was determined in the analysis of inclusive

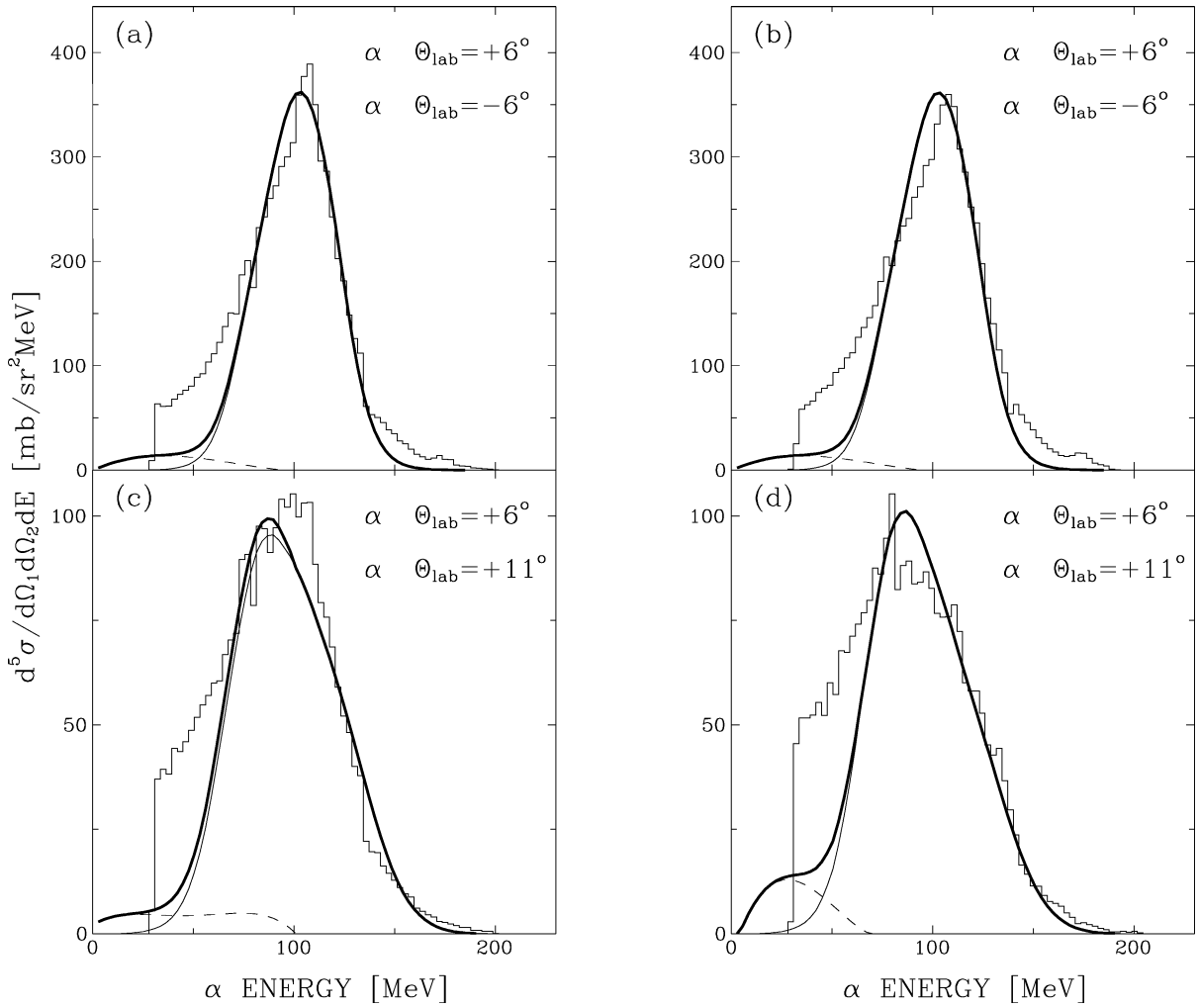

FIG. 13. Experimental $\alpha-\alpha$ coincidence spectra compared with results of calculations for various processes. Thin solid lines: sequential process leading to three or six α particles in the final state; thin dashed lines: α particles evaporated from compound nucleus; thick solid lines: sum of these processes.

α particle and ^{12}C ejectile distributions. The values of the parameters $\delta=\epsilon=\cdots=0.06$ MeV^{-1} were used for processes in which decay occurs in two or more steps. They were fixed according to the dependence of the experimental coincidence cross section on the excitation energy for four body reactions leading to $\alpha-^{7}$Be, $\alpha-^{7}$Li, and $\alpha-^{6}$Li coincidences. To obtain absolute values of the cross sections the normalization factor N was adjusted separately for each reaction channel. Then the total cross section for each analyzed sequential process may be calculated by integration of the calculated distributions over solid angle and over the energy of the outgoing particle. The choice of the values of the parameters β, γ, δ, ... was not very critical for the results of the analysis. For example, variation of $\gamma_{\text{inel.}}$ parameter (for sequential processes started by inelastic excitation) in $0.03-0.05$ MeV^{-1} range as well as β parameter in $0.1-0.2$ deg^{-1} range leads to a very similar description of the experimental data. These uncertainties of parameters determination cause that the cross sections for various sequential processes were estimated with an error of about 15%.

The kinematical considerations taking into account all experimental data enabled to determine which reaction processes are significant and should be taken into account in a detailed quantitative analysis. They are listed in Table I. The quality of data description may be judged using as examples the coincidence cross sections for $\alpha-^{9}$Be, $\alpha-^{6}$Li, $\alpha-\alpha$ and the inclusive cross sections for all the channels.

$\alpha-^{9}$Be coincidences. The main contribution to these coincidences is due to the three body reaction ^{12}C(^{12}C,α^{9}Be)^{11}C and to the deuteron transfer reaction followed by proton and α particle emission $^{12}\text{C}+^{12}\text{C}\rightarrow\alpha+^{9}\text{Be}+p+^{10}\text{B}$. Coincidence cross sections were evaluated for these two sequential reactions in the frame of our phenomenological model. The only free parameters were the normalization factors for both reactions determined from the simultaneous analysis of coincidence and inclusive data. The contributions of different processes are compared with experimental coincidence spectra in Fig. 10. The sum of cross sections for both these sequential mechanisms together with a contribution from compound nucleus reactions reproduces the experimental coincidence data very well, with exception of small angle of α particle emission.

$\alpha-^{6}Li$ coincidences. Kinematical considerations presented in the previous chapter lead to the conclusion that ^{6}Li nuclei are produced mainly in the following sequential processes: Inelastic excitation of ^{12}C nucleus followed by the

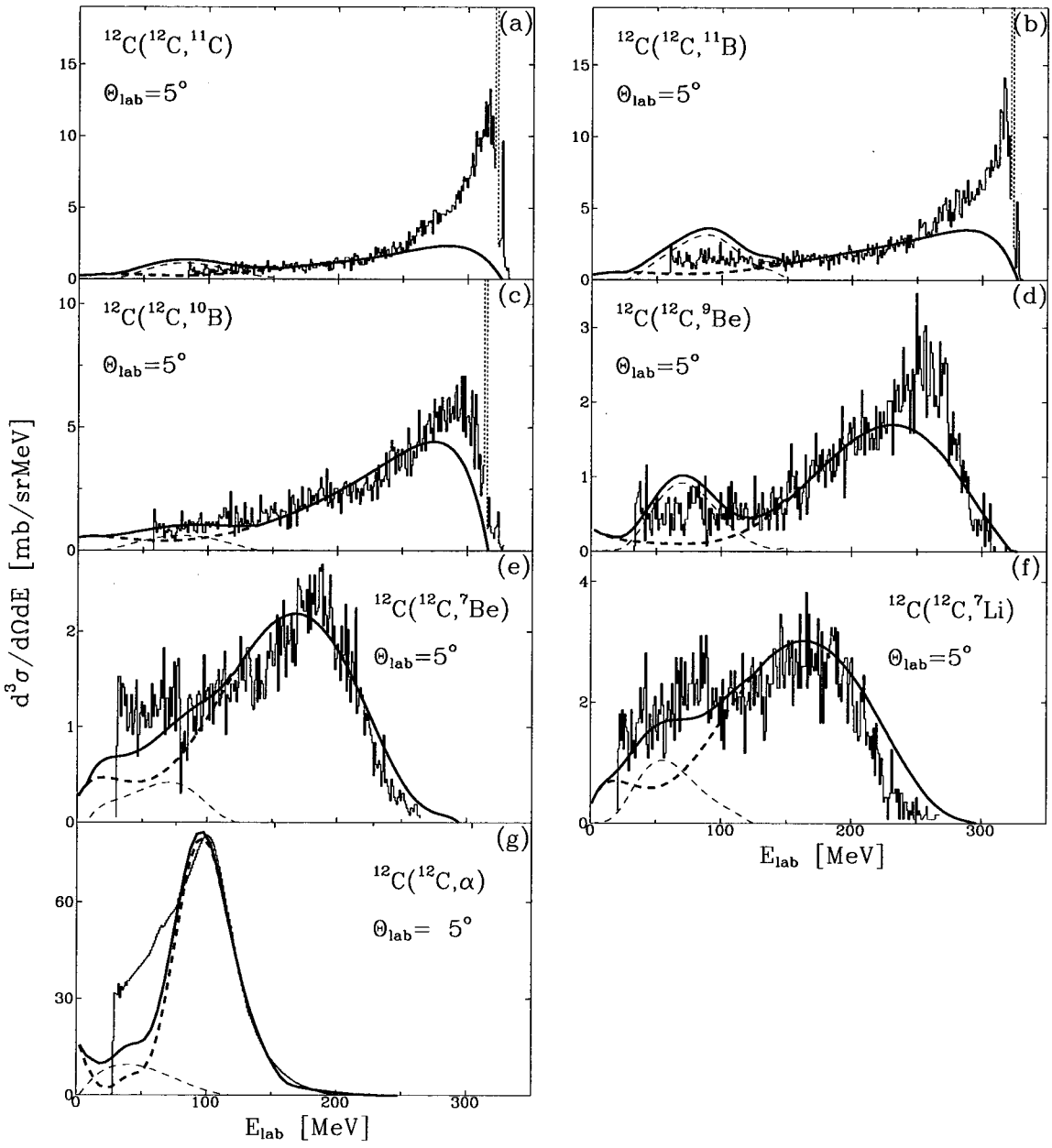

FIG. 14. Experimental inclusive spectra for laboratory angle $\theta_{lab}=5°$ for ^{11}C, ^{11}B, ^{10}B, ^{9}Be, ^{7}Be, ^{7}Li, and α ejectiles. The thick dashed lines represent the sum of the cross sections for corresponding sequential processes given in Table I, thin dashed lines correspond to compound nucleus calculations, and thick solid lines represent the sum of cross sections for these reactions.

decay chain $^{12}C^{*}\rightarrow d+^{10}B^{*}\rightarrow d+^{6}Li+\alpha$ or $^{12}C^{*}\rightarrow p+^{11}B^{*}\rightarrow p+n+^{10}B^{*}\rightarrow n+p+^{6}Li+\alpha$ or $^{12}C^{*}\rightarrow n+^{11}C^{*}\rightarrow n+p+^{10}B^{*}\rightarrow p+n+^{6}Li+\alpha$. Contribution of the first mechanism to the experimental coincidence cross sections is shown in Fig. 11 as thick dashed line while the contribution from the other ones is presented as thin solid line. All mechanisms contribute significantly to the reaction under consideration. The normalization factors can be determined unambigously by taking into account also inclusive spectra. From the inclusive spectra presented in Fig. 12 it is obvious that contribution of four body reactions decreases quickly with the scattering angle. Therefore the normalization for the five body reactions can be obtained from fitting the inclusive spectra at large scattering angles. As can be seen from Fig. 11 the sum of the contributions from the sequential and compound nucleus reactions reproduces well the experimental coincidence data.

$\alpha-\alpha$ coincidences. It may be stated from inspection of Table I that the α particle inclusive cross section is the most important contribution to the total reaction cross section. Therefore it is essential to obtain a good model description of the reactions in which α particles emerge. From the sequential processes listed in Table I only the inelastic excitation of ^{12}C nucleus followed by decay into three α particles may lead to $\alpha-\alpha$ coincidences. The kinematical analysis of $\alpha-\alpha$ coincidences allows the conclusion that the decay of ^{12}C nucleus into three α particles proceeds sequentially with the production of the intermediate ^{8}Be nucleus. It was as-

sumed in the analysis that the ^{8}Be nucleus is produced in the ground state and the first excited state only. The complex analysis of α particle spectra and $\alpha-\alpha$ coincidences allows the determination of the normalization factor N and relative strength of the production of ^{8}Be nuclei in the ground and first excited states. It was found that ^{8}Be nuclei are produced in both these states with the same probability. The quality of the model description of $\alpha-\alpha$ coincidences is illustrated by Fig. 13 where the experimental spectra (histograms) for two angular configurations are compared with model results (thick solid line).

The inclusive spectra. They are very well reproduced by model calculations in the whole measured angular range for all ejectiles. This is shown in Fig. 12 for ^{6}Li energy spectra for several angles and in Fig. 14 where energy spectra of other ejectiles measured at $\theta_{\rm lab}=5°$ has been collected. It is seen that sequential fragmentation processes account for a large part of the experimental cross section and together with the cross section for the compound nucleus describe very well the experimental spectra (solid line in Fig. 14). Part of the ^{11}C and ^{11}B spectra at high energies not reproduced by sequential processes corresponds to one nucleon transfer reactions analyzed separately in Refs. [15,18,19]. Total cross sections for each sequential process derived from the analysis are given in Table I.

The very good description of experimental data obtained in the quantitative analysis permits to accomplish a balance of the total reaction cross section. The obtained total inelastic excitation cross section followed by the decay was found to be 800 mb. In the inelastic excitation process both interacting nuclei are mutually excited to energies larger than the decay threshold. The mutual excitation accounts for about 75% of the inelastic excitation cross section. The sequential processes started by transfer give 200 mb. Therefore, the total cross section for the sequential fragmentation processes was estimated to be 1000 mb. The cross section for compound nucleus reaction was found to be 200 mb. The experimental cross section corresponding to two body processes (integrated cross section for measured discrete state transitions) is equal to about 40 mb. All these processes combined give the total cross section value of 1240 mb with an estimated error of about 200 mb which agrees very well with the total reaction cross section of 1290 mb obtained from the optical model calculations. Thus the sequential processes started by direct reactions may account for about 80% of the total reaction cross section, 5% have to be attributed to the direct processes with ejectiles being in bound states whereas fusion is responsible for about 15%.

VI. CONCLUSIONS

The reaction mechanism for the $^{12}C+^{12}C$ system was studied at an intermediate energy of 28.7 MeV/nucleon. The performed experiment containing measurements of both inclusive as well as coincidence spectra with good (Z,A) identification enabled a detailed analysis of the data.

The analysis of the experimental coincidence spectra based on kinematical considerations indicates that the reaction mechanism is dominated by sequential three, four, and five body processes. A phenomenological model for a quantitative description of the data was formulated. The application of this model led to very good reproduction of the coincidence and inclusive data and thus delivered information on absolute values of cross sections.

The accomplished balance of cross sections shows that in the energy region under investigation the sequential processes started by direct reactions together with the contribution from the compound nucleus reaction mechanism and direct reactions exhaust almost completely the total reaction cross section.

[1] L. G. Moretto and G. J. Wozniak, Annu. Rev. Nucl. Part. Sci. **43**, 379 (1993).
[2] H. Fuchs and K. Möhring, Rep. Prog. Phys. **57**, 231 (1994).
[3] F. Saint-Laurent, Nucl. Phys. **A583**, 481 (1995).
[4] K. Hagel, M. Gonin, R. Wada, J. B. Natowitz, F. Haddad, Y. Lou, M. Gui, D. Utley, B. Xiaó, J. Li, G. Nebbia, D. Fabris, G. Prete, J. Ruiz, D. Drain, B. Cheynis, D. Duinet, X. C. Hu, A. Demeyer, C. Pastor, A. Giorni, A. Lleres, P. Stassi, J. B. Viano, and P. Gonthier, Phys. Rev. C **50**, 2017 (1994).
[5] D. Heuer, A. Chabane, M. E. Brandan, M. Charvet, A. J. Cole, P. Désesquelles, A. Giorni, A. Lleres, A. Menchaca-Rocha, J. B. Viano, D. Benchekroun, B. Cheynis, A. Demeyer, E. Gerlic, D. Guinet, M. Stern, and L. Vagneron, Phys. Rev. C **50**, 1943 (1994).
[6] E. Bauge, A. Elmaani, Roy A. Lacey, N. N. Ajitanand, D. Craig, M. Cronqvist, E. Gualtieri, S. Hannuschke, T. Li, B. Llope, T. Reposeur, A. Vander Molen, G. D. Westfall, J. S. Winfield, J. Yee, S. Yennello, A. Nadasen, R. S. Tickle, and E. Norbeck, Phys. Rev. Lett. **70**, 3705 (1993).
[7] T. Li, W. Bauer, D. Craig, M. Cronqvist, E. Gualtieri, S. Hannuschke, R. Lacey, W. L. Llope, T. Reposeur, A. M. Vander Molen, G. G. Westfall, W. K. Wilson, J. S. Winfield, J. Yee, S. J. Yennello, A. Nadasen, R. S. Tickle, and E. Norback, Phys. Rev. Lett. **70**, 1924 (1993).
[8] S. J. Yenello, K. Kwiatkowski, E. C. Pollacco, C. Volant, Y. Cassagnou, R. Dayras, D. E. Fields, S. Harar, E. Hourani, R. Legrain, E. Norbeck, R. Planeta, J. L. Wile, N. R. Yoder, and V. E. Viola, Phys. Rev. C **48**, 1092 (1993).
[9] K. Hagel, M. Gonin, R. Wada, J. B. Natowitz, B. H. Sa, Y. Lou, M. Gui, D. Utley, G. Nebbia, D. Fabris, G. Prete, J. Ruiz, D. Drain, B. Chambon, B. Cheynis, D. Guinet, X. C. Hu, A. Demeyer, C. Pastor, A. Giorni, A. Lleres, P. Stassi, J. B. Viano, and P. Gonthier, Phys. Rev. Lett. **68**, 2141 (1992).
[10] D. A. Cebra, S. Howden, J. Karn, A. Nadasen, C. A. Ogilvie, A. Vander Molen, G. D. Westfall, W. K. Wilson, J. S. Winfield, and E. Norbeck, Phys. Rev. Lett. **64**, 2246 (1990).
[11] D. Pelte, U. Winkler, M. Gnirs, A. Gobbi, K. D. Hildenbrand, and R. Novotny, Phys. Rev. C **39**, 553 (1989).
[12] W. Terlau, M. Bürgel, A. Budzanowski, H. Fuchs, H. Homeyer, G. Röschert, J. Uckert, and R. Vogel, Z. Phys. A **330**, 303 (1988).
[13] J. Pouliot, Y. Chan, D. E. DiGregorio, B. A. Harmon, R.

Knop, C. Moisan, R. Roy, and R. G. Stokstad, Phys. Rev. C **43**, 735 (1991).

[14] E. Chavez-Lomeli, A. Dacal, M. E. Ortiz, S. B. Gazes, Y. Chan, R. G. Stokstad, E. Plagnol, K. Siwek-Wilczynska, and J. Wilczynski, Phys. Rev. C **48**, 699 (1993).

[15] L. Jarczyk, B. Kamys, A. Magiera, R. Siudak, A. Strzałkowski, B. Styczeń, J. Hebenstreit, W. Oelert, P. von Rossen, H. Seyfarth, and G. R. Satchler, Nucl. Phys. **A518**, 583 (1990).

[16] J. Czudek, I. Jarczyk, B. Kamys, A. Magiera, R. Siudak, A. Strzałkowski, B. Styczeń, J. Hebenstreit, W. Oelert, P. von Rossen, H. Seyfarth, A. Budzanowski, and A. Szczurek, Phys. Rev. C **43**, 1248 (1991).

[17] A. Szczurek, A. Budzanowski, L. Jarczyk, A. Magiera, K. Möhring, R. Siudak, and T. Srokowski, Z. Phys. A **338**, 187 (1991).

[18] L. Jarczyk, B. Kamys, A. Magiera, Z. Rudy, A. Strzałkowski, B. Styczeń, J. Hebenstreit, W. Oelert, P. von Rossen, and H. Seyfarth, Z. Phys. A **342**, 169 (1992).

[19] R. Siudak, Ph.D. thesis, Jagellonian University, Cracow, 1993.

[20] A. Magiera, Institute of Nuclear Physics, Cracow 1996, Report No. 1732/PL.

[21] A. Gavron, in *Computational Nuclear Physics 2*, edited by K. Langanke, J. A. Maruhn, and S. E. Koonin (Springer-Verlag, New York, 1993), p. 108.

[22] A. Gilbert and A. G. W. Cameron, Can. J. Phys. **43**, 1446 (1965).

[23] T. D. Newton, Can. J. Phys. **34**, 804 (1956).

[24] L. Jarczyk, B. Kamys, J. Okołowicz, J. Sromicki, A. Strzałkowski, H. Witała, Z. Wróbel, M. Hugi, J. Lang, R. Müller, and E. Ungricht, Nucl. Phys. **A325**, 510 (1979).

[25] M. Kistryn, L. Jarczyk, B. Kamys, A. Magiera, Z. Rudy, A. Strzałkowski, R. Barná, V. D'Amico, D. De Pasquale, A. Italiano, and M. Licandro, Phys. Rev. C **54**, 1720 (1996).

[26] L. C. Vaz, J. M. Alexander, and G. R. Satchler, Phys. Rep. **69**, 373 (1981).

[27] L. Jarczyk, B. Kamys, A. Magiera, J. Sromicki, A. Strzałkowski, G. Willim, Z. Wróbel, D. Balzer, K. Bodek, M. Hugi, J. Lang, R. Müller, and E. Ungricht, Nucl. Phys. **A369**, 191 (1981).

[28] F. Porto and S. Sambatoro, Nuovo Cimento A **83**, 339 (1984).